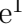


V994 Her: A Unique Triply Eclipsing Sextuple Star System

P. Zasche¹ *, T. Borkovits^{2,3,4,5,6}, R. Jayaraman⁷, S. A. Rappaport⁷, M. Brož¹,
D. Vokrouhlický¹, I. B. Bíró^{2,3}, T. Hegedüs², Z. T. Kiss², R. Uhlař⁸,
H. M. Schwengeler⁹, A. Pál⁴, M. Mašek¹⁰, S. B. Howell¹¹, S. Dallaporta¹²,
U. Munari¹³, R. Gagliano¹⁴, T. Jacobs¹⁵, M. H. Kristiansen^{16,17}, D. LaCourse¹⁸,
M. Omohundro¹⁹, I. Terentev²⁰, A. Vanderburg²¹, Z. Henzl^{22,23}, B. P. Powell²⁴,
V. B. Kostov^{24,25,26}

¹ Charles University, Faculty of Mathematics and Physics, Astronomical Institute, V Holešovičkách 2, Praha 8, 180 00, Czech Republic

² Baja Astronomical Observatory of Szeged University, H-6500 Baja, Szegedi út, Kt. 766, Hungary

³ ELKH-SZTE Stellar Astrophysics Research Group, H-6500 Baja, Szegedi út, Kt. 766, Hungary

⁴ Konkoly Observatory, Research Centre for Astronomy and Earth Sciences, H-1121 Budapest, Konkoly Thege Miklós út 15-17, Hungary

⁵ ELTE Gothard Astrophysical Observatory, H-9700 Szombathely, Szent Imre h. u. 112, Hungary

⁶ MTA-ELTE Exoplanet Research Group, H-9700 Szombathely, Szent Imre h. u. 112, Hungary

⁷ MIT Department of Physics and MIT Kavli Institute for Astrophysics and Space Research, Cambridge, MA 02139, USA

⁸ Private Observatory, Pohorčí 71, 254 01 Jílové u Prahy, Czech Republic

⁹ Citizen Scientist, Planet Hunter, Bottmingen, Switzerland

¹⁰ FZU - Institute of Physics of the Czech Academy of Sciences, Na Slovance 1999/2, CZ-182 21, Praha, Czech Republic

¹¹ NASA Ames Research Center, Moffett Field, CA 94035, USA

¹² ANS Collaboration, c/o Astronomical Observatory, 36012 Asiago (VI), Italy

¹³ INAF Astronomical Observatory of Padova, 36012 Asiago (VI), Italy

¹⁴ Amateur Astronomer, Glendale, AZ 85308

¹⁵ Amateur Astronomer, 12812 SE 69th Place Bellevue, WA 98006, USA

¹⁶ 3DTU Space, National Space Institute, Technical University of Denmark, Elektrovej 327, DK-2800 Lyngby, Denmark

¹⁷ Brorfelde Observatory, Observator Gyldenkerne Vej 7, DK-4340 Tållzse, Denmark

¹⁸ Amateur Astronomer, 7507 52nd Place NE Marysville, WA 98270, USA

¹⁹ Citizen Scientist, c/o Zooniverse, Department of Physics, University of Oxford, Denys Wilkinson Building, Keble Road, Oxford, OX1 3RH, UK

²⁰ Citizen Scientist, Planet Hunter, Petrozavodsk, Russia

²¹ Kavli Institute for Astrophysics and Space Research, Massachusetts Institute of Technology, Cambridge, MA 02139, USA

²² Hvězdárna Jaroslava Trnky ve Slaném, Nosačická 1713, Slaný 1, 274 01, Czech Republic

²³ Variable Star and Exoplanet Section, Czech Astronomical Society, Fričova 298, 251 65 Ondřejov, Czech Republic

²⁴ NASA Goddard Space Flight Center, 8800 Greenbelt Road, Greenbelt, MD 20771, USA

²⁵ SETI Institute, 189 Bernardo Ave, Suite 200, Mountain View, CA 94043, USA

²⁶ GSF Sellers Exoplanet Environments Collaboration

Accepted XXX. Received YYY; in original form ZZZ

ABSTRACT

We report the discovery with *TESS* of a third set of eclipses from V994 Herculis (TIC 424508303), previously only known as a doubly-eclipsing system. The key implication of this discovery and our analyses is that V994 Her is the second fully-characterized (2+2) + 2 sextuple system, in which all three binaries eclipse. In this work, we use a combination of ground-based observations and *TESS* data to analyze the eclipses of binaries A and B in order to update the parameters of the inner quadruple’s orbit (with a derived period of 1062 ± 2 d). The eclipses of binary C that were detected in the *TESS* data were also found in older ground-based observations, as well as in more recently obtained observations. The eclipse timing variations of all three pairs were studied in order to detect the mutual perturbations of their constituent stars, as well as those of the inner pairs in the (2+2) core. At the longest periods they arise from apsidal motion, which may help constraining parameters of the component stars’ internal structure. We also discuss the relative proximity of the periods of binaries A and B to a 3:2 mean motion resonance. This work represents a step forward in the development of techniques to better understand and characterize multiple star systems, especially those with multiple eclipsing components.

Key words: binaries: eclipsing – binaries: close – stars: individual: (TIC 424508303, V994 Her), sextuple system

1 INTRODUCTION

Multiple star systems consisting of three or more stars are estimated to make up at least 30% of binaries, based on a statistical analysis of Kepler data in [Borkovits et al. \(2016\)](#). However, only two thousand have been observed in detail, and the number of systems known with multiplicities higher than 5 is $\lesssim 50$ ([Tokovinin 2018](#)). Understanding these high-multiplicity systems is important, as they can shed new light on many of the open questions that remain in currently-accepted models of stellar formation and provide insight into the dynamical interactions of multiple stars ([Aarseth & Mardling 2001](#)).

V994 Herculis (V994 Her, TIC 424508303) is a bright, well-studied quadruple system, with two known eclipsing binary components ([Lee et al. 2008](#)). At the time, this was the first known doubly-eclipsing quadruple system. The component stars are bright and massive, and the periods of the two eclipsing binary components have been well-constrained: binary A consists of a B8V and an A0V star, with a period of 2.083 days; binary B consists of an A2V and an A4V star, with a period of 1.420 days. These stars are young and occupy a position near the zero-age main sequence (ZAMS) on the Hertzsprung-Russell (H-R) diagram.

[Martín-Ruiz et al. \(2013\)](#) initially postulated, based on analyses of photometric data, that this system could harbor another eclipsing binary. However, because the quality of their data was rather poor, with relatively low photometric precision, their results were not conclusive enough. With the advent of high-precision space-based survey missions such as the Transiting Exoplanet Survey Satellite (*TESS*; [Ricker et al. 2015](#)), we are able to conclusively confirm the presence of a third set of eclipses using the *TESS* light curves. Table 1 contains basic information about V994 Her and a nearby visual companion (separated by $\approx 1''$).

[Zasche & Uhlař \(2016\)](#) were the first to accurately constrain the period of the inner binaries’ (A and B) revolution about their common center of mass ($\simeq 1060$ days in their study). Additionally, they argued that TIC 1685970000, a faint ($m_V \sim 8.8$) neighbor some $1.1''$ away from V994 Her, is also gravitationally bound to the main quadruple, making it one of the few known quintuple star systems. This putative close companion has been observed many times since its discovery as a visual double in 1831, and these measurements have been catalogued in the Washington Double Star Catalog (WDS; [Mason et al. 2001](#)). The WDS calls the known quadruple a “primary star,” and the fainter companion a “secondary star.” However, any physical connection between these two visually-close objects has not yet been conclusively proven; further follow-up and analyses (such as those in Section 5.1) can resolve this question.

In this paper, we introduce V994 Her as a bona fide triply eclipsing sextuple star system, which we identified using *TESS* data. In addition to the known set of two binaries, the system also consists of a third binary of period 1.96 days, and we demonstrate that the visual companion listed in the WDS catalog is likely gravitationally bound to the primary star. In Section 2, we describe all available observational data and how they were prepared and used for the analysis. Then, Section 3 provides detailed modelling of the available data, while 4 discusses the results of our modeling. Finally, in Section 5 we discuss the possible architecture of the whole system

Table 1. Archival properties of the V994 Her visual double star

Name	V994 Her TIC 424508303	TYC 2110-1170-2 TIC 1685970000
RA (J2000, deg)	276.941222	276.941246
Dec (J2000, deg)	24.697407	24.697757
<i>TESS</i> ^a	7.037 ± 0.017	8.3949 ± 0.6
<i>B</i> ^a	7.136 ± 0.024	
<i>V</i> ^a	6.9599 ± 0.023	
<i>J</i> ^a	6.948 ± 0.019	
<i>H</i> ^a	6.999 ± 0.0036	
<i>K</i> ^a	6.989 ± 0.023	
<i>W1</i> ^b	6.844 ± 0.07	
<i>W2</i> ^b	6.838 ± 0.02	
<i>W3</i> ^b	6.903 ± 0.018	
<i>W4</i> ^b	6.732 ± 0.067	
<i>G</i> ^c	7.0966	8.8761
<i>G</i> _{Bp} ^c	6.9898	6.9842
<i>G</i> _{Rp} ^c	6.9358	6.9869
Parallax ^c (mas)	3.43639 ± 0.08394	3.48065 ± 0.09849
PM ^c (RA, mas/yr)	5.5770 ± 0.0701	4.8802 ± 0.1275
PM ^c (Dec, mas/yr)	11.2675 ± 0.0765	7.1568 ± 0.0834

Notes: Magnitudes are from (a) TIC-8 catalog ([Stassun et al. 2019](#)), (b) WISE point source catalog ([Cutri et al. 2021](#)), (c) *Gaia* DR3; PM stands for proper motion ([Gaia Collaboration et al. 2022](#)). Some parameters for the visual companion TIC 1685970000 are difficult to come by, as the brighter primary star is $1.1''$ away from it, making measurements difficult.

that we infer from our findings and comment on the proximity of the inner 2+2 component (binaries A and B) to their mutual 3:2 mean motion resonance.

2 OBSERVATIONS OF V994 HER

2.1 *TESS* Observations

V994Her was observed by *TESS* during Year 2 in Sector 26 (i.e., June 2020), and during Year 4 in Sectors 40 and 53 (i.e. July 2021 & June 2022). In Sector 26, this star was observed at 2-minute cadence; this light curve was pre-processed and detrended by the Science Processing Operations Center (SPOC) pipeline ([Jenkins et al. 2016](#)), which is partially based on that used for Kepler data. The detrended SPOC light curve from Sector 26 is shown in Figure 1. For the Year 4 observations, however, only the full-frame image (FFI) data (at 10-minute cadence) are available. These data were processed using the convolution-based differential image analysis methods of the *fitsh* package ([Pál 2012](#)). V994 Her’s triply eclipsing nature was identified both algorithmically and through a visual survey¹ of all stars brighter than 13.5 mag in the *TESS* FFIs (for more information on the latter initiative, see [Kristiansen et al. 2022](#)).

2.1.1 Three methods for disentangling

Using the *TESS* data, we applied three different methods to disentangle the combined light curve into the three component eclipsing signals: the time-domain iterative disentangle-

¹ This search makes use of the LcTools desktop application ([Schmitt et al. 2019](#)) to view and study light curves.

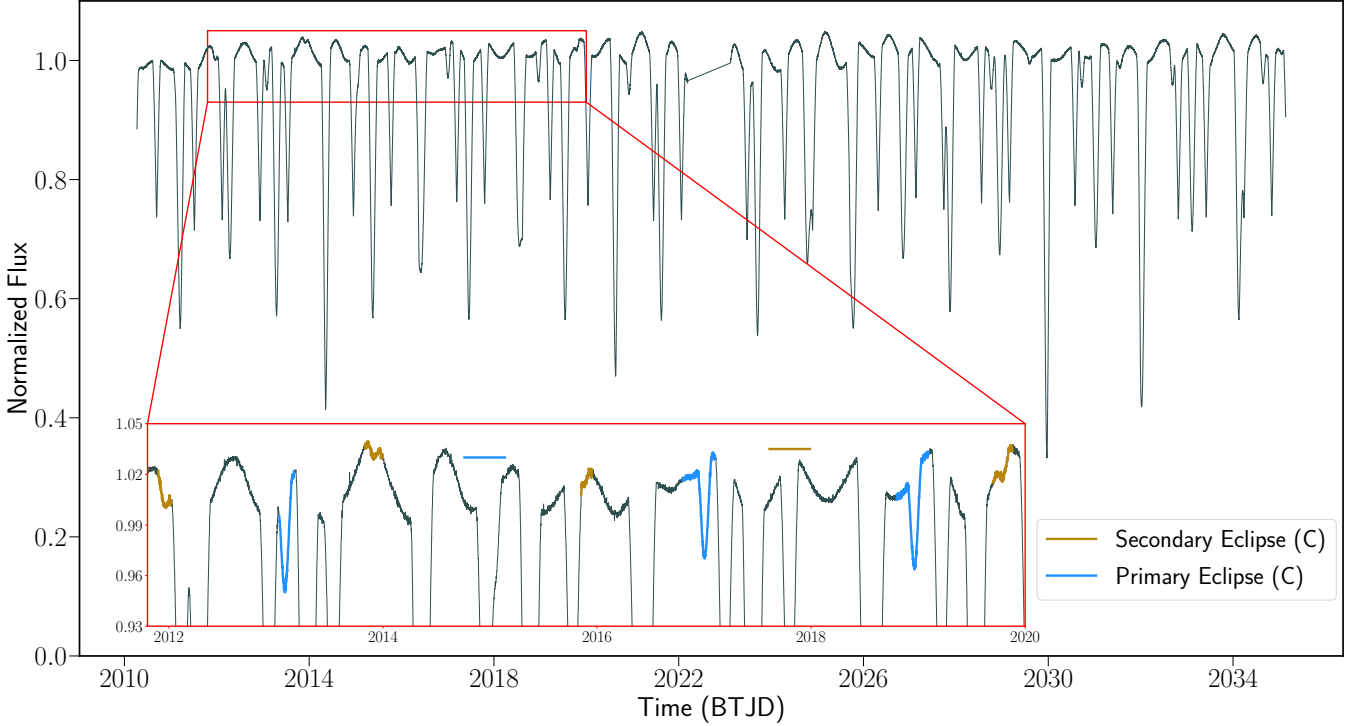


Figure 1. The *TESS* Sector 26 light curve of TIC 424508303, aka V994 Her. The x-axis is plotted in Barycentric *TESS* Julian Day (BTJD), which corresponds to BJD–2457000.0. The main plot shows the full 25-day light curve, which includes multiple eclipses from the previously known eclipsing binaries A and B (Lee et al. 2008; Zasche & Uhlář 2016). It also contains relatively shallow eclipses from the new binary C, discussed in this work. The inset panel shows a zoom-in on a roughly 9-d segment of the data. Three clearly visible primary eclipses of the C binary are overplotted in blue, while the eclipse lost in a deeper eclipse from the A binary is indicated with a blue line above its expected location. The (shallow) secondary eclipses of the C binary are overplotted in gold, with the gold line at BTJD \sim 2017.8 indicating a secondary eclipse that is lost in one of the deeper eclipses from the “main” quadruple.

ment method, the Fourier-decomposition method, and the iterative phenomenological model method. Results for all three methods are plotted side-by-side in Figure 2.

First, we used the method of time-domain iterative disentanglement. This technique is a powerful tool for separating the light curves of strongly blended targets, and was described in detail in Section 3 of Powell et al. (2021), where it was applied for the first time to disentangle the blended light curves of three eclipsing binaries.

To verify our results and compare the three methods, we used two other methods to disentangle the light curves. The second one is the Fourier-based iterative method, which was also described in Section 3.1 of Powell et al. (2021). Such a technique is suitable for these data because all the signals of interest are strictly periodic over at least one sector of *TESS* data, wherein movement on the longer outer orbit can be neglected. The third and final method is based on iteratively fitting the individual pairs with their respective phenomenological models and then subtracting these from the overall light curve. After a few (usually two to five) iterative steps, a shape for the eclipsing light curve of the C pair was clearly obtained. The method itself and the code used here are described in the Appendix of Pejcha et al. (2022).

Apart from the three eclipsing signals, the light curve also exhibits an additional pulsation-like oscillation. Such a variation shows a periodicity of $(P_A - P_B)$. This extra feature is apparently not present in the Fourier-disentangled light

curve, as well as in the phenomenologically-disentangled one (see the bottom panels of Figure 2). This may be due to the subtraction of this signal as part of the disentanglement process. Unfortunately, we have not yet been able to come up with a coherent astrophysical explanation of this signal.

We found the first method of time-domain iterative disentanglement as the most suitable for a subsequent analysis of the individual light curves, which is discussed in Section 3. This is mainly due to problematic fitting of outside-eclipse parts of the light curves by the methods 2 and 3.

To derive the precise times of eclipses of each binary, we used the result of the time-domain iterative disentanglement method. These were calculated for each binary after subtraction of the light curves of the other two pairs. Eclipse times of each binary, as observed in *TESS*, are presented in Tables A1, A2, and A3.

2.2 Ground-based photometric Observations

2.2.1 Baja Astronomical Observatory, Hungary (2007)

V994 Her was observed with the 50-cm f/6 modified Cassegrain Baja Astronomical Robotic Telescope (BART-1), located at the Baja Astronomical Observatory in Hungary, on 40 nights between 18 June 2007 and 9 October 2007. The observations were carried out with a 4096×4096 Apogee Alta U16 CCD camera, using a standard Johnson V filter.

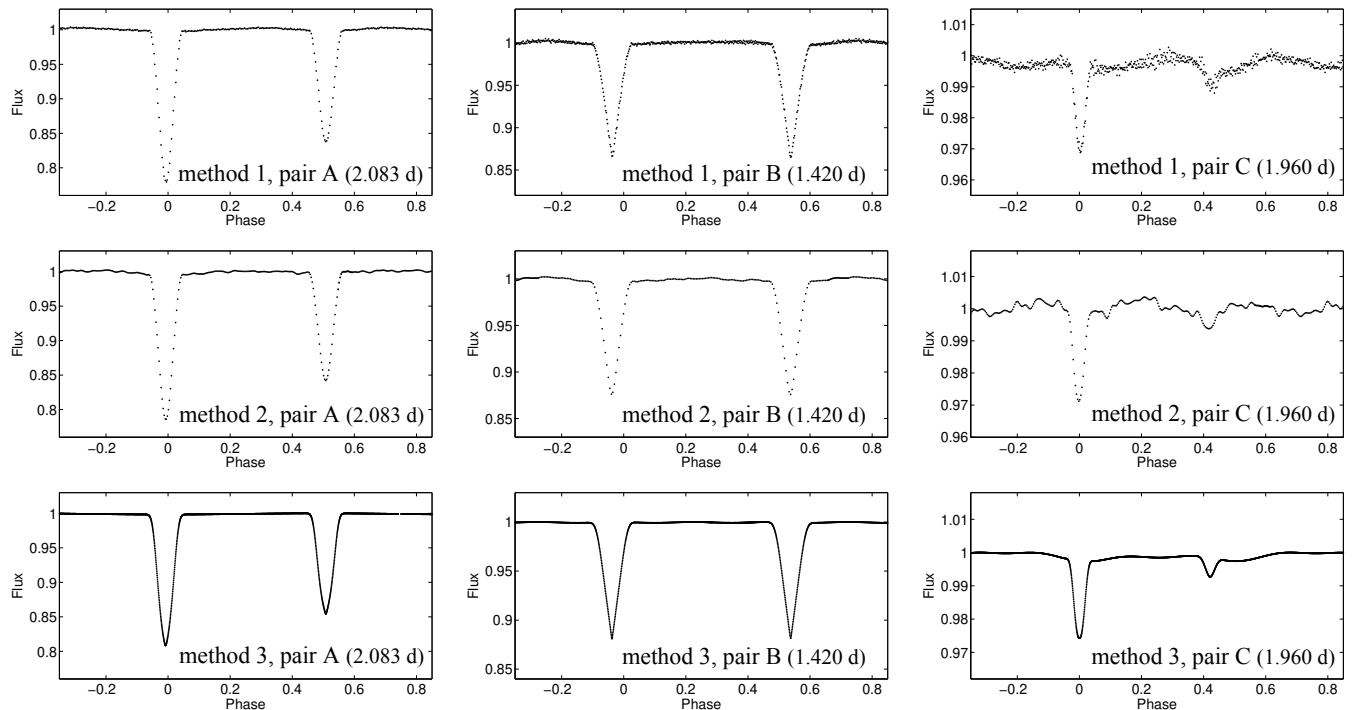


Figure 2. The disentangled and folded light curves of all three eclipsing binaries A, B, and C using different approaches: the time-domain iterative disentanglement (i.e. method 1), the Fourier-decomposition (method 2), and the iterative phenomenological model methods (method 3), respectively. For details see the text.

The original goal of this photometric monitoring of V994 Her was to prove and publish for the first time the previously-unknown doubly eclipsing nature of this system; however, Lee et al. (2008) independently discovered and characterized this system’s true nature. Thus, our team at the time chose to not further analyze the data and simply published the derived times of minima in Borkovits et al. (2011). However, we make use of this archival photometric data set in the present work, as it is especially useful for an additional constraining of the apsidal advance rates of binaries A and B through the complete lightcurve fittings and, also for checking the constancy (or variability) of the eclipse depths within a one and half decade-long interval.

2.2.2 Additional observations

V994 Her was monitored over several dozens of nights by R.U. at his private observatory in the Czech Republic, as well as remotely from northern Italy using three different telescopes: a 34-mm refractor, a 150-mm reflector, and a 200-mm reflector. Some of these observations were obtained using filtered photometry (usually with R or I filters), while others were carried out without any filter. Due to the different instrumental setups of these instruments, the comparison stars were different for each telescope; however, they were always chosen to be adequately close to the target and of a similar spectral type in order to minimize the effect of differential extinction during the nights. Additionally, four more nights of data were obtained by the 250-mm F/(Ph)otometric Robotic Atmospheric Monitor (FRAM) telescope CTA-N, located on the island of La Palma, Spain (Prouza et al. 2019). We also have data from one night of observations by M.M. at his

private observatory in the Czech Republic, using a 200-mm reflector. From the combination of these datasets, more than 40 new times of eclipses for pair A were derived, and more than 30 for pair B. Several new estimates for pair C were also calculated; however, these are of lower quality due to the significantly lower photometric amplitude of its variation.

Between 2002 June 10 and 2004 July 14, a total of 1170 measurements in V -band and 653 in B -band were collected for V994 Her by S.D. and U.M., using a 28-cm telescope located in Cembra (Trento, Italy). This telescope was equipped with an Optec SSP-5 photoelectric photometer and Johnson B and V filters. The comparison and check stars were, respectively, HIP 89975 ($V = 6.978$ mag, $B - V = -0.095$ mag) and HIP 90637 ($V = 5.862$ mag, $B - V = -0.099$ mag). These stars are nearly identical in $B - V$ color to V994 Her and are located nearby on the sky ($\leq 2^\circ$ angular separation). From these data, we were also able to derive several times of eclipses for both the A & B pairs. Moreover, we were able to derive a rough value for the times of eclipse for pair C, which allowed us to significantly improve our estimate of its orbital period due to the increased time coverage.

All the previously-unpublished eclipse times are given in Table A4. The minima presented in this work for the first time, as well as the previously-published ones, were used for a final fit of the data over the whole interval (covering more than 30 years now). This is shown in Figure 3 for all three pairs.

2.3 Other Catalogs

We queried the WDS Catalog for archival data on V994 Her and its nearby visual companion (TIC 1685970000), with

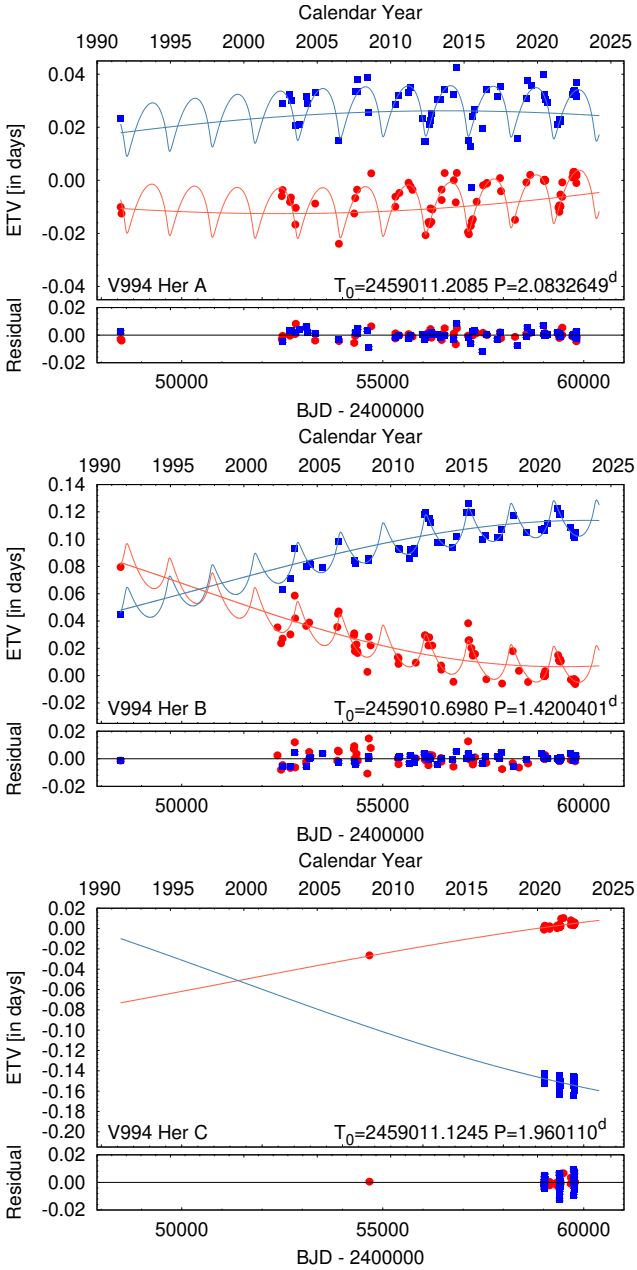


Figure 3. Eclipse timing variations (ETVs) of V994 Her collected over the past three decades, with the *TESS* eclipses included. The top, middle and bottom panels show the ETVs for binary A, B and C, in that order; the red and blue points denote the primary and secondary eclipses, respectively. The red and blue curves are the photodynamical fitting models. The “divergence” of the ETVs for the primary and secondary eclipses are due to apsidal motion.

measurements spanning from 1831 to 2015. This data consisted of position angles and separations for the system between these years. Additionally, we calculated the position angle and separation for the visual double using data from *Gaia* DR3 (Gaia Collaboration et al. 2022). These data were used in Section 5.1 to investigate whether or not the visual double star is gravitationally bound.

Table 2. System parameters derived from speckle imaging^a.

Parameter	Value
obs. date [JD]	2459710.018 ± 0.001
position angle [deg]	357.5 ± 0.5
separation [arc sec]	1.06 ± 0.01
δV [mag] ^b	1.89 ± 0.2
δI [mag] ^b	1.67 ± 0.2

Notes: (a) Observations made at 562 nm and 832 nm with the ‘Alopeco speckle interferometric imager mounted on the Gemini North 8-m telescope (Scott et al. 2021). (b) Difference in magnitude between Image 1 (containing binaries A and B) and Image 2 (likely hosting binary C).

2.4 Speckle observation

V994 Her was observed on 10 May 2022 using the, ‘Alopeco speckle interferometric imager mounted on the Gemini North 8-m telescope (Scott et al. 2021). ‘Alopeco provides simultaneous speckle imaging in two bands (562 nm and 832 nm), with output data products including a reconstructed image and derived parameters for any detected close companion stars. Three sets of 1000×0.06 sec exposures were collected; these underwent Fourier analysis in the standard reduction pipeline (Howell et al. 2011).

Figure 4 shows the image around V994 Her, with a bright component to the South (hereafter ‘Image 1’) which hosts binaries A and B. The fainter image to the North (hereafter ‘Image 2’) is $1.06''$ away, and we believe that this image hosts binary C, as discussed in Section 5.1. At the 290 pc distance to V994 Her (derived from the *Gaia* DR3 parallax), this corresponds to a spatial separation of ~ 307 au. The middle panel shows a zoom-in around Image 1, revealing that there are no resolved components within it, down to a limiting resolution of $\lesssim 0.1''$. Both the image of the quadruple system to the South (Image 1), and binary C (likely residing in Image 2) remain unresolved into their component parts—respectively, either the A and B binaries, and the primary and secondary star in binary C—as these components are separated on the sky by less than our 20 mas nominal angular resolution. This value is the Gemini optical diffraction limit when Nyquist sampled with $2 \times 0.01''$ pixels. Our derived $5\text{-}\sigma$ contrast curves for this observation, for both the 562 nm and 832 nm images, are shown in the bottom panel. These curves will be further discussed in Sect. 5.1 as we attempt to rule out the possibility that binary C might actually be located in Image 1.

The system properties gleaned from the speckle observations are summarized in Table 2.

3 PHOTODYNAMICAL MODELING

We carried out a joint photodynamical modeling in which we combined the three sectors of *TESS* data alongside the 2007 *V* band Baja light curves. As part of this, we also modeled the eclipse timing variation (ETV) curves of all three binaries, the radial velocity (RV) points of binaries A and B obtained by Lee et al. (2008), and the net stellar spectral energy distributions (SEDs). To prepare for this analysis, we improved the LIGHTCURVEFACTORY software package to allow it to handle hierarchical configurations of (2+2)+2 stars in their entirety. Specifically, the updated code calculates the

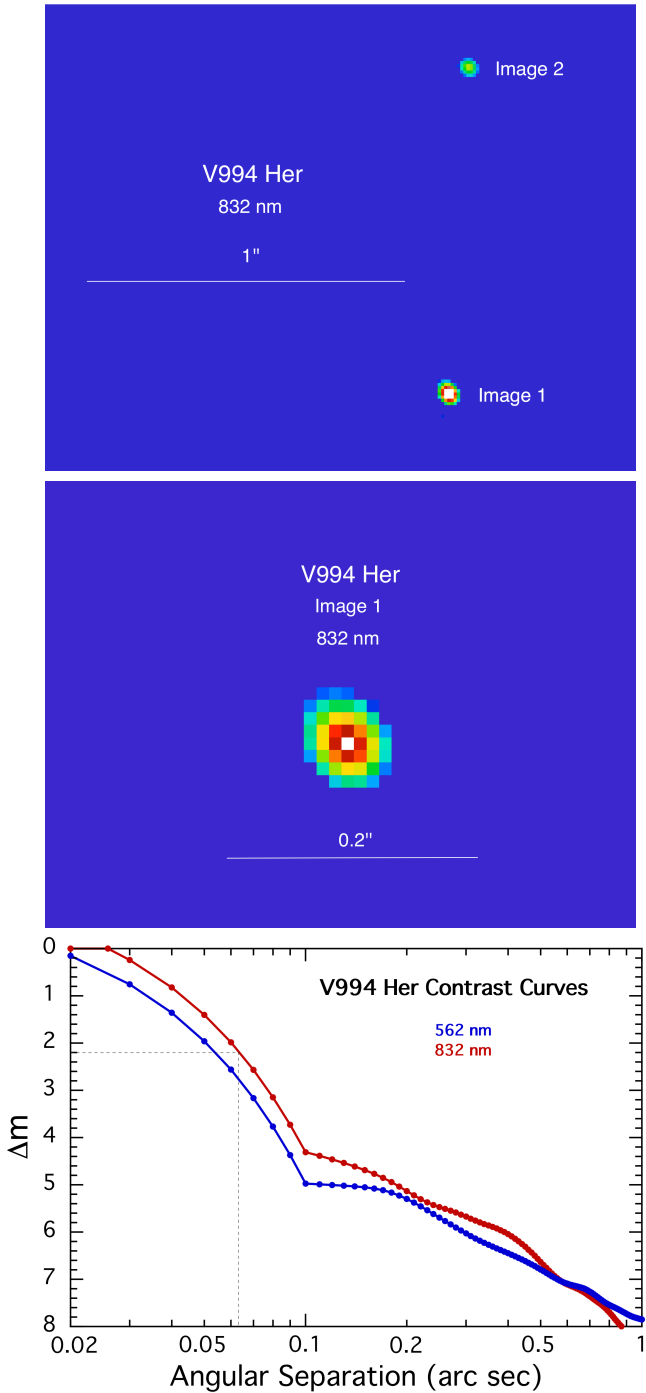


Figure 4. Speckle imaging of V994 Her. North is up and East is to the left. *Top panel:* 832 nm image of a $1.5'' \times 1.5''$ region near V994 Her. We define the brighter feature to the South as ‘Image 1,’ which contains binaries A and B. We label the ~ 1.7 magnitude fainter object to the North as ‘Image 2’. *Middle panel:* Same as top panel but zoomed in around Image 1. Each pixel is $0.01''$ in size. *Bottom panel:* $5\text{-}\sigma$ confidence level contrast curves (obtained at 562 nm and 832 nm). The image spans angular scales from the diffraction limit, near 20 mas, out to $\sim 1''$, the approximate end of speckle coherence. The dotted black lines mark the detectable separation distance of $\sim 0.06''$ of a source that is 2.2 magnitudes fainter than Image 1 itself (i.e., the approximate brightness of binary C).

revolutions of the six bodies on their three inner orbits, the middle orbit (i.e., of the quadruple), and the outer orbit (i.e., of the sextuple). All five orbits may be considered either to be purely Keplerian or, for tight systems, LIGHTCURVEFACTORY is able to take into account the mutual perturbations of the constituent stars with numerical integration of the orbital motions. Moreover, any combinations of two-body or multiple-body eclipses are also considered. The updated code does not require the disentangling of the three eclipsing binary light curves; rather, they can be modeled in their observed, blended form (e.g., as shown in Figure 1). Apart from this improvement, the software package is functionally identical to that described in previous work (see, e.g., Borkovits et al. 2019, 2021).

For the specific case of V994 Her, we find that binaries A and B form a relatively wide 2+2 quadruple system ($P_{A-B}/P_B > P_{A-B}/P_A > 500$). As a result, the gravitational perturbations of the binary components in the 2+2 quadruple are small and can be described by simple Keplerian orbits. Therefore, we use a simple analytic Keplerian formalism in order to calculate the stellar positions at any given time, with the slight empirical modification of considering, for all three binaries, a constant apsidal advance rate ($\dot{\omega}_{A,B,C}$) and reference values for the argument of periastron ($\omega_{A,B,C}$) at a specific epoch. A physical interpretation of the apsidal motion is discussed in Section 4.1.

In our joint photodynamical analysis, we optimized the following parameters using a Markov Chain Monte Carlo (MCMC) method:

(i) Orbit-related parameters:

- For all four orbits (three eclipsing pairs and the quadruple A-B): The components of the eccentricity vectors at epoch t_0 : $(e \sin \omega)_{A,B,C,A-B}$, $(e \cos \omega)_{A,B,C,A-B}$, and the inclinations relative to the plane of the sky: i_A , i_B , i_C , i_{A-B} .
- For the A–B orbit: the period P_{A-B} and the periastron passage time τ_{A-B} .
- For the three eclipsing pairs: the (constant) apsidal advance rates: $\dot{\omega}_{A,B,C}$.

(ii) Stellar parameters:

- Six mass-related parameters: the masses of the primaries ($m_{Aa,Ba,Ca}$), and the mass ratios of the three EBs ($q_{A,B,C}$),
- The metallicity of the system ($[M/H]$),
- The (logarithmic) age of the six coeval stars ($\log \tau$),
- The interstellar reddening $E(B - V)$, and
- The “extra light” contamination (ℓ) parameters.

A couple of other parameters were constrained instead of being adjusted or held constant during our analyses:

(i) Orbits:

- The sidereal orbital periods of the inner binaries ($P_{A,B,C}$) and their respective orbital phases (derived using the time of an arbitrary primary eclipse) were constrained internally through the ETV curves.
- The systemic radial velocity of the whole sextuple system (γ) is calculated a posteriori at the end of each trial step by minimizing the value of χ^2_{RV} .

Note that the (2+2)+2 mode of LIGHTCURVEFACTORY

requires the orbital elements of the outermost (AB-C) orbit. In the present case, this orbit is completely unknown. We do know, however, that it must be so wide that we do not expect any observable variations in the positions of the six stars arising from their motion along this orbit. Thus, we chose the elements of this outermost orbit arbitrarily; we use a circular orbit seen face-on with a period of ~ 30 kyr with its parameters kept fixed.

(ii) Stars:

- The radii and temperatures of the six stars were calculated with the use of three linear interpolations from the precomputed 3D PARSEC grids (the dimensions were metallicity, logarithmic age, and stellar mass).
- The distance of the system (needed for the SED fitting) was calculated a posteriori at the end of each trial step, by minimizing the value of χ^2_{SED} . For a detailed explanation of this process, see Borkovits et al. (2020).

The atmospheric parameters of the stars were handled in a similar manner as in our previous photodynamical studies. We utilized a logarithmic limb-darkening law (Klinglesmith & Sobieski 1970), for which the passband-dependent linear and non-linear coefficients were interpolated in each trial step via the tables from the original version of the *Phoebe* software (Prša & Zwitter 2005). We set the (constant) gravity darkening exponents for five radiative stars to $\beta = 1$; for the coolest, solar-like component Cb, however, we used $\beta = 0.32$, which is in line with the classical model of Lucy (1967) and is valid for convective stars.

Prior to conducting our analysis, we performed some further preparatory steps on the light curves. First, after disentangling the three eclipsing binaries as in Section 2.1.1, we found that the residual *TESS* light curves contained oscillations with an amplitude of approximately 2% and a characteristic period of $(P_A - P_B)$. We removed this oscillation from the light curves before performing the full photodynamical analysis by subtracting the final residual light curve of the iterative disentanglement process (which contained this periodic variability) from the original *TESS* light curves for each sector. Second, for the sake of equal sampling across sectors, we binned the 2-min sector 26 *TESS* light curve to 10-min bins, identical to the cadence time of the sector 40 and 53 FFI light curves. We also binned the 2007 Baja photometry to 10-min bins. Third, we noticed that the eclipse depths of all three binaries in sector 26 were deeper by a few percent than the corresponding eclipses in the sectors 40 and 53 data; the depths in the latter two sectors were similar. As a result, we assume that in sector 26, the ratio of contaminating light is somewhat lower than in the other two sectors. Thus, for the sector 26 light curve, we adjusted the amount of contaminating light independent of sectors 40 and 53. The effect of slightly different flux contamination for the same star in data from different *TESS* sectors has been studied previously in the literature (see, e.g., Plachy et al. 2021.)

The median values and their $1\text{-}\sigma$ uncertainties (derived from the MCMC calculation) for the orbital and physical parameters of the sextuple system, as well as some derived quantities, are tabulated in Table 3. Furthermore, a comparison of the observed and model light curves are plotted in Figure 5, while a similar comparison for the ETV curves is

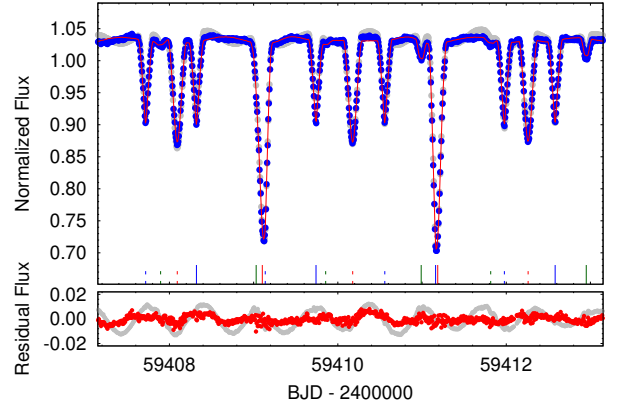


Figure 5. A section of the *TESS* sector 40 light curve (blue points) after the removal of the oscillations with period $(P_A - P_B)$, plotted with the photodynamically fitted model light curve (red). We also plot the original light curve, including the oscillations with period $P_A - P_B$, using gray points. The short vertical solid and dashed lines along the x-axis, colored red, blue and green, denote the mid-eclipse times of the primary and secondary eclipses of binaries A, B and C, respectively. The residual curves are shown below the main light curve.

shown in Figure 3. Note that Table 3 presents the absolute physical parameters for the C binary and both its components, despite the fact that we do not have any directly observed radial velocities for this pair. However, we have the RVs of both the A and B binaries as well as changes of the RVs on their mutual orbit. We can consequently derive the properties of this binary by using the LIGHTCURVEFACTORY code to combine the light curve modeling of the C binary and the SED of the overall system.

4 THE FINAL PARAMETERS

Our thorough modeling of the system also yields the position of each star in the H-R diagram. Due to the fact that the age of the system was also taken as a free parameter (under the assumption that all six stars are coeval), we can characterize its evolutionary state. From the calculated value of the system's logarithmic age (presented in Table 3), the system is rather young and therefore located close to the ZAMS. This is in agreement with the fact that all of the orbits are slightly eccentric, so the circularization process is still ongoing (see, e.g., Claret & Cunha 1997).

Only a few sextuple systems have well-constrained parameters, including their masses and orbital elements; as a result, it is not very easy to compare V994 Her with others. Interestingly, the recent analysis of the sextuple system TIC 168789840 (Powell et al. 2021) revealed a vastly different configuration, wherein all three binary pairs have similar mass ratios. In V994 Her, our analysis suggests that all three components have very different mass ratios. Perhaps V994 Her is more similar to the well-known Castor system, which has a similar architecture, with its component binaries having very different mass ratios (see, e.g., Tokovinin 2018).

The whole system is plausibly close to a co-planar configuration, given the inclination angles in Table 3. However, to

Table 3. Median values of the parameters from the joint spectro-photodynamical analysis of (i) all three EB light curves, (ii) both sets of radial velocities from the SB2 (i.e., the quadruple consisting of binaries A and B), (iii) all three sets of ETVs, and (iv) joint SED and PARSEC evolutionary tracks.

Parameter	Binary A		Binary B		Binary C		A-B orbit
P_a [days]	2.0832039 ^{+0.0000042} _{-0.0000039}		1.4200981 ^{+0.0000033} _{-0.0000040}		1.9601064 ^{+0.0000018} _{-0.0000018}		1062.3 ^{+2.8} _{-2.4}
a [R_\odot]	11.85 ^{+0.17} _{-0.11}		8.30 ^{+0.07} _{-0.05}		9.45 ^{+0.17} _{-0.23}		910 ⁺¹² ₋₈
i^a [deg]	84.66 ^{+0.33} _{-0.33}		89.19 ^{+0.63} _{-0.62}		80.42 ^{+2.39} _{-0.99}		83 ⁺⁴ ₋₅
e	0.0276 ^{+0.0010} _{-0.0010}		0.1186 ^{+0.0007} _{-0.0007}		0.1893 ^{+0.0052} _{-0.0046}		0.687 ^{+0.050} _{-0.037}
ω [deg]	208.4 ^{+3.4} _{-4.3}		174.7 ^{+2.4} _{-2.7}		314.0 ^{+3.4} _{-2.3}		59.6 ^{+3.6} _{-3.9}
$\dot{\omega}$ [deg/yr]	1.86 ^{+0.42} _{-0.55}		3.66 ^{+0.17} _{-0.16}		1.68 ^{+0.24} _{-0.24}		—
τ [BJD - 2 400 000]	59 010.855 ^{+0.020} _{-0.025}		59 010.393 ^{+0.009} _{-0.011}		59 009.306 ^{+0.007} _{-0.007}		58 166.8 ^{+13.6} _{-9.3}
$t_{\text{prim eclipse}}$ [BJD - 2 400 000]	59 011.1821 ^{+0.0014} _{-0.0019}		59 010.7324 ^{+0.0028} _{-0.0021}		59 011.1246 ^{+0.0004} _{-0.0004}		—
q ($= m_2/m_1$)	0.757 ^{+0.008} _{-0.009}		1.009 ^{+0.009} _{-0.009}		0.583 ^{+0.104} _{-0.074}		0.738 ^{+0.017} _{-0.013}
K_{pri} [km s ⁻¹]	124 ⁺² ₋₂		150 ⁺¹ ₋₁		90 ⁺¹¹ ₋₈		25 ⁺² ₋₁
K_{sec} [km s ⁻¹]	163 ⁺² ₋₂		148 ⁺¹ ₋₁		154 ⁺⁸ ₋₇		34 ⁺³ ₋₂
γ [km/s]	—		—		—		-38.7 ^{+0.3} _{-0.3}
individual stars	Aa	Ab	Ba	Bb	Ca	Cb	
Relative Quantities:							
fractional radius ^b [R/a]	0.1785 ^{+0.0022} _{-0.0026}	0.1452 ^{+0.0013} _{-0.0015}	0.1895 ^{+0.0019} _{-0.0019}	0.1903 ^{+0.0018} _{-0.0017}	0.1648 ^{+0.0038} _{-0.0039}	0.1016 ^{+0.0198} _{-0.0106}	
fractional luminosity in <i>TESS</i> -band	0.3822 ^{+0.0099} _{-0.0143}	0.1847 ^{+0.0073} _{-0.0072}	0.1227 ^{+0.0029} _{-0.0022}	0.1258 ^{+0.0029} _{-0.0025}	0.1086 ^{+0.0199} _{-0.0107}	0.0145 ^{+0.0113} _{-0.0055}	
fractional luminosity in <i>V</i> -band	0.4115 ^{+0.0169} _{-0.0175}	0.1909 ^{+0.0098} _{-0.0115}	0.1184 ^{+0.0041} _{-0.0054}	0.1220 ^{+0.0047} _{-0.0056}	0.1021 ^{+0.0227} _{-0.0163}	0.0085 ^{+0.0074} _{-0.0035}	
extra light [ℓ_{S26}]	—		0.0576 ^{+0.0155} _{-0.0221}		—		
[$\ell_{S40,53}$]	—		0.1808 ^{+0.0141} _{-0.0215}		—		
[ℓ_V]	—		0.0366 ^{+0.0334} _{-0.0256}		—		
Physical Quantities:							
T_{eff}^c [K]	11890 ⁺³¹⁰ ₋₂₆₄	9915 ⁺²⁵⁶ ₋₂₀₁	8832 ⁺¹⁵⁸ ₋₁₅₆	8895 ⁺¹⁷⁵ ₋₁₇₀	8514 ⁺⁵¹⁴ ₋₃₁₀	5893 ⁺⁴⁵¹ ₋₃₈₄	
mass [M_\odot]	2.929 ^{+0.124} _{-0.093}	2.216 ^{+0.106} _{-0.070}	1.913 ^{+0.050} _{-0.040}	1.889 ^{+0.055} _{-0.049}	1.810 ^{+0.169} _{-0.072}	1.077 ^{+0.162} _{-0.109}	
radius ^c [R_\odot]	2.118 ^{+0.026} _{-0.030}	1.721 ^{+0.038} _{-0.031}	1.572 ^{+0.028} _{-0.019}	1.579 ^{+0.027} _{-0.018}	1.544 ^{+0.071} _{-0.035}	0.961 ^{+0.199} _{-0.115}	
luminosity ^c [L_\odot]	80.2 ^{+10.4} _{-7.7}	25.7 ^{+3.9} _{-2.6}	13.5 ^{+1.1} _{-1.0}	14.1 ^{+1.3} _{-1.2}	11.2 ^{+4.4} _{-1.8}	1.00 ^{+0.94} _{-0.41}	
[M_{bol}]	0.01 ^{+0.11} _{-0.13}	1.25 ^{+0.12} _{-0.16}	1.94 ^{+0.09} _{-0.09}	1.90 ^{+0.10} _{-0.09}	2.15 ^{+0.19} _{-0.36}	4.77 ^{+0.57} _{-0.72}	
$\log g^c$ [cgs]	4.252 ^{+0.017} _{-0.013}	4.312 ^{+0.005} _{-0.005}	4.321 ^{+0.007} _{-0.007}	4.321 ^{+0.007} _{-0.007}	4.317 ^{+0.009} _{-0.007}	4.503 ^{+0.065} _{-0.103}	
$\log(\text{age})$ [dex]	—		7.92 ^{+0.12} _{-0.23}		—		
[M/H] [dex]	—		0.073 ^{+0.042} _{-0.056}		—		
$E(B-V)$ [mag]	—		0.050 ^{+0.011} _{-0.014}		—		
$(M_V)_{\text{tot}}$	—		-0.30 ^{+0.07} _{-0.07}		—		
distance [pc]	—		274 ⁺⁶ ₋₆		—		

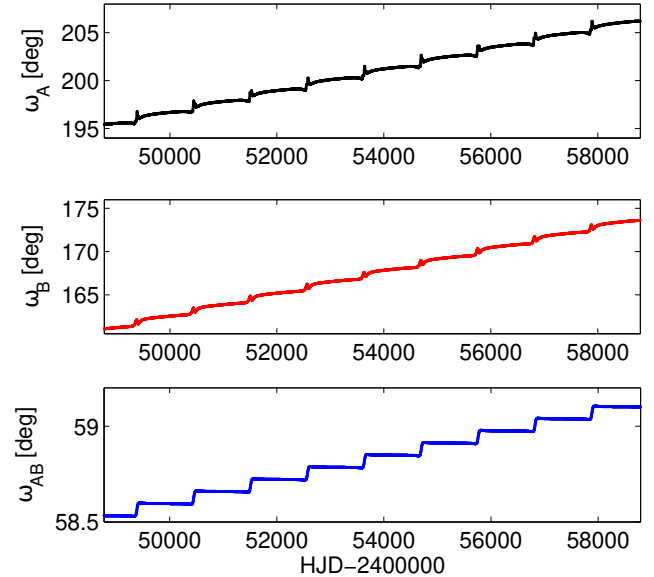
Notes: (a) Calculated only from the $\sin i$ terms; (b) Polar radii; (c) Interpolated from the PARSEC isochrones

derive its true orbital architecture we would also need to calculate the values for the longitude of the ascending node Ω . To do so, one would need to derive a precise interferometric orbit, which is not available to us currently. Once this information is obtained, we can speculate whether or not the system can exhibit Kozai-Lidov cycles (Kozai 1962; Lidov 1962); however, these may be halted anyway by rapid precession of the pericenters of the component binaries (Table 3 and Vokrouhlický 2016, for an example).

4.1 Apsidal motion

Given that we have multiple high-precision sets of eclipse times (see Tables A1, A2, A3, and A4), and that each binary has an eccentric orbit, we are able to derive apsidal motion rates for all three pairs in the system. We find that this rate is approximately a few degrees per year, suggesting that their apsidal advance is not at all negligible. In order to properly interpret these empirically fitted rates, we first have to subtract any contributions from the apsidal advance that can be accurately computed.

First, we determine the relativistic contribution to the observed apsidal motion (see, e.g., Claret & Giménez 2010). Given the orbital and physical parameters in Table 3 we find this effect represents about 10%, 8%, and 6% of the total for the binaries A, B, and C, respectively. Because these percentages are rather small, we can consider all three sub-systems of

**Figure 6.** Results of the numerical modeling of the orbits of binaries A and B and the quadruple AB. Here, we show the long-term evolution of the arguments of periastron (without the tidal term). Pair A is plotted in black; pair B, in red; and their mutual orbit (A-B), in blue. See section 4.1 for details.

V994 Her as classical apsidal rotators, rather than relativistic ones.

Because the inner 2+2 component of binaries A and B is not too wide, there also exists a classical (Newtonian) contribution to their apsidal motion, arising from mutual dynamical perturbations between A and B. In order to estimate this effect, we ran a simulation using the N-body code developed by Brož (2017) and Brož et al. (2022). For the sake of definiteness, we assumed a nearly-coplanar system configuration by imposing identical initial values of the nodal longitude for both the A and B orbits, with other orbital parameters taken from Table 3. We found that such mutual perturbations in the A and B system account for another 12% and 5% of the total apsidal motion in the respective component (see Figure 6, which shows these contributions). The binary C is deemed to be distant enough from the A and B binaries so that we do not provide the classical apsidal contribution in this case.

With those two effects estimated and subtracted from the total values of the observed apsidal motions in the A, B and C systems, we can assume that the remainder is attributable to the effect of the stellar tidal interactions. From these rates of $\dot{\omega}_{\text{tidal}}$, one can usually derive the internal structure constants and compare them with theoretical ones from stellar evolution models (e.g. Claret 2004). However, when comparing the results for pair B (which has the best coverage of its apsidal period, since it has the fastest rate), our resulting values deviate slightly from the predicted theoretical ones. The tidal contribution to the apsidal rate was found to be $\dot{\omega}_{\text{tidal,B}} = (3.14 \pm 0.20)$ deg/yr, yielding an internal structure constant of $\log k_2 = -2.44 \pm 0.05$, while the theoretical models of Claret (2004) suggest that its value should be -2.36 ± 0.02 . In order for the respective error intervals to overlap, one needs to have either larger uncertainties in the derived parameters, a slightly faster apsidal motion (of about 5%), subsynchronous rotation of the component stars (about 20% slower), or a combination of all three of these effects. Another way to account for this discrepancy is by using the fact that these stars, found to be very young, were likely born in a metal-rich environment. Using the stellar evolution models of Claret (2007) with a higher metallicity ($Z=0.04$), we find $\log k_2 = -2.40 \pm 0.02$, which is in much better agreement with the observed value of $\log k_2$.

The N-body modelling also allows us to estimate the apsidal advance of the quadruple orbit A-B (shown in Figure 6). This motion – accumulating to $\sim 0.6^\circ$ over the interval of available observations – is orders of magnitude slower when compared to the values for the A and B systems. However, over the next few decades, when the change will have cumulatively added up to a few degrees, one can readily detect such movement with newly obtained data. On the other hand, other effects such as the change in orbital inclination and eclipse depth would still be negligible on such a timescale.

We also note that the eccentric orbits of the inner binaries are subject to the circularization effect. From the theory of circularization by Zahn (1977) and equations by Claret & Cunha (1997) the appropriate circularization time scales are of the order of magnitude longer than the estimated age of the system as resulted from our modelling.

5 DISCUSSION

5.1 V994 Her and its visual companion

In the prior sections, we conclusively demonstrated the presence of a third eclipsing binary in the V994 Her system. Here, we discuss the likelihood that binary C is hosted by Image 2 (fainter object to the North, as seen in Fig. 4), as well as the probability that Image 2 is physically bound to Image 1. If so, this would give the system a (2+2)+2 configuration.

According to the photodynamical fit for the system parameters presented in Table 3, binary C has 14% the light of binaries A+B in the *TESS* band, and 13% in *V* band. That corresponds to magnitude differences of 2.1 and 2.2, respectively, in the *TESS* and *V* bands. The bottom panel of Fig. 4 suggests that these contrasts correspond to being able to resolve two objects within Image 1 (the brighter southerly object) that are separated by $\gtrsim 0.06''$. Since both Images 1 and 2 are 290 pc away, the resolvable physical separation at this magnitude contrast would correspond to 18 au. The actual semimajor axis of the binary A and B quadruple, which resides in Image 1, is 4.2 au (see Table 3). It is always possible, of course, that at the time of the speckle observations, the projected distance between the center of light of binaries A+B and a putative close orbiting neighbor (i.e., binary C) might inadvertently be very small due to unlucky orbital phasing. Let us assume, however, for the sake of argument, that A+B and C are at some nominal separation on the sky at this particular outer orbital phase when the speckle measurements were made. In that case, the outer orbit of C around A+B, within Image 1, would have to have a semimajor axis of not much more than ~ 20 au before it is resolvable.

For a stable triple system (i.e., C stably orbiting A+B) the ratio of semi-major axes must satisfy

$$a_{\text{out}} \gtrsim 2.8 \left(\frac{M_{\text{ABC}}}{M_{\text{AB}}} \right)^{2/5} \frac{(1 + e_{\text{out}})^{2/5}}{(1 - e_{\text{out}})^{6/5}} a_{\text{in}}, \quad (1)$$

where equation (1) is from Rappaport et al. (2013), which in turn is based on the work of Mardling & Aarseth (2001) and Mikkola (2008). If we take as a very rough estimate that $a_{\text{out}} \lesssim 20$ au, and we know that $a_{\text{in}} \sim 4.2$ au, then we find a constraint on e_{out} such that

$$\frac{(1 + e_{\text{out}})^{2/5}}{(1 - e_{\text{out}})^{6/5}} \lesssim 1.5. \quad (2)$$

In turn, this requires that $e_{\text{out}} \lesssim 0.25$. Thus, while this is not an unreasonably small value for an outer orbital eccentricity, we can see from this exercise, that there is “not much room to spare” in trying to fit binary C into an orbit about binaries A+B, all *within* Image 1. Furthermore, recall that the contrast limits shown in Fig. 4 are 5- σ limits. Thus, we tentatively conclude that binary C, in fact, is hosted by Image 2 (the fainter one to the North).

We next look at the question of whether Image 2 (likely containing binary C) is physically bound to Image 1 (hosting binaries A and B). For this analysis, we have two pieces of kinematic evidence: (i) the proper motions of Images 1 and 2 from Gaia DR3 (Gaia Collaboration et al. 2022), and (ii) the historical astrometric data, spanning 200 years, of the WDS catalog (Mason et al. 2001). This information is summarized in Table 4, and the WDS astrometric data are plotted in Fig. 7.

The two proper motion results (Gaia and WDS) evaluated

Table 4. Observational Kinematics Between Image 1 and Image 2

Cartesian motion ^a	mas yr ⁻¹	km s ⁻¹
Gaia PM RA	-0.70 ± 0.14	-0.96 ± 0.20
WDS ^b PM RA	-1.22 ± 0.10	-1.68 ± 0.14
Gaia PM Dec	-4.11 ± 0.11	-5.66 ± 0.16
WDS ^b PM Dec	-3.84 ± 0.35	-5.29 ± 0.48
angular motion	—	—
WDS ^{b,c} \dot{r} [mas yr ⁻¹]	-3.86 ± 0.35	—
WDS ^{b,c} $\dot{\theta}$ [mrad yr ⁻¹]	-1.10 ± 0.09	—

Notes: (a) Image 2 value - Image 1. (b) Washington Double Star catalog (Mason et al. 2001). (c) These refer to the rate of change in the separation and the position angle, respectively, and are inferred from the fits shown in Fig. 7.

at the Gaia epoch are in agreement on the proper motion of the declination (PM Dec) to better than 1σ , while the proper motions of the right ascension (PM RA) differ by 2.9σ . We attribute this discrepancy to fitting a linear function to $\dot{\theta}^2$ over a 200 year interval. The total relative velocity between Image 1 and Image 2 on the plane of the sky is in the range 5.55 – 5.74 km s⁻¹ depending on whether we choose to use the WDS or Gaia results, respectively.

To check whether Image 2 is physically bound to Image 1, we take the escape speed to be

$$v_{\text{esc}} \simeq \sqrt{\frac{2GM_{\text{ABC}}}{s}}, \quad (3)$$

where M_{tot} is the total mass contained in Image 1 plus Image 2, and s is the instantaneous (3D) separation of Image 1 and Image 2. As representative values, we estimate $M_{\text{ABC}} = M_A + M_B + M_C = 11.5 M_{\odot}$ from Table 3, and $s \gtrsim 307$ au, where the latter is the physical separation on the plane of the sky between Image 1 and Image 2. This leads to an estimate for $v_{\text{esc}} \lesssim 8.2$ km s⁻¹. Since this value is substantially larger than the relative speed of Image 1 vs. Image 2 (at least in the plane of the sky), we tentatively take this as strong evidence that the Image 1 plus Image 2 system is physically bound. However, we remain unsure about the relative speed and separation in the direction along our line of sight.

Finally, we make another independent argument which also strongly suggests that Image 1 and Image 2 are physically bound. This argument relies on the fact that Image 2 is found so close in the sky to Image 1, with similar proper motions and distance, and the two are not too dissimilar in magnitude. We seek to quantify the relative occurrence rate of such a pair of stars. Using Gaia data, we searched for other stars with similar properties to those of Image 2. In particular, we looked for stars that have (i) PM RA within an absolute value of 1 mas yr⁻¹ of image 1; (ii) PM Dec with absolute value within 5 mas yr⁻¹ of Image 1; (iii) a parallax within absolute value of 0.2 compared to Image 1; and (iv) having a G magnitude brighter than 9. When we search the Gaia database for other stars that satisfy these criteria, we find 13 such stars within 30° of Image 1. Given that the search area is $\sim 10^{10}$ times larger than the area needed to include Image 2 (at $1''$ distance from Image 1), we conclude that Image 1,

² $\dot{\theta} \equiv$ rate of change in the position angle.

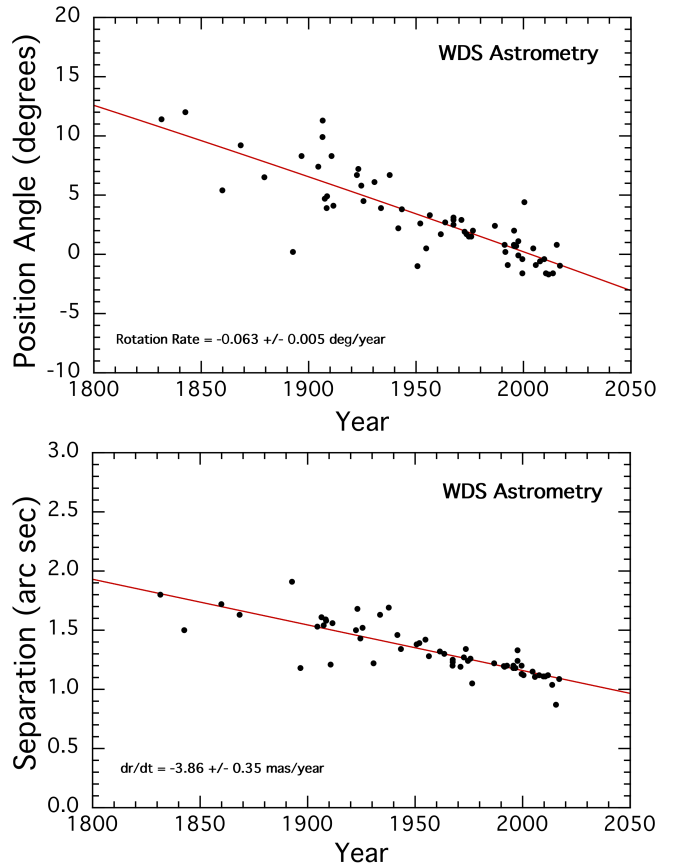


Figure 7. A plot of position angle and separation for the two stars in the visual binary catalogued by the Washington Double Star catalog (Mason et al. 2001) at the position of V994 Her.

with its given properties, is not remotely likely to be found there by accident.

The conclusion from the above argument is that either Image 2 is physically bound to Image 1, or it is comoving with it by virtue of having been born in the same stellar nursery. The latter scenario can be ruled out rather readily. We have seen that the relative speed between Image 1 and Image 2 (on the plane of the sky) is 5.6 km s⁻¹. The age of the system (from Table 3) is $\simeq 60$ Myr. If the two images were unbound and merely approximately comoving on the sky, then during that time the two images would have drifted apart in the ensuing 60 Myr by some 300 pc. This is much, much larger than the current sky separation of 290 au. Thus, we conclude that Image 2 is physically bound to Image 1.

Given the above discussion, we believe that the most likely configuration of this sextuple is a (2+2)+2 system, with the inner quadruple system containing binaries A and B situated in Image 1, and the third binary (C) in Image 2. There is also a slim chance, but not yet fully ruled out, that Image 1 hosts all three binaries, and Image 2 represents a 7th star or yet another binary (‘D’). The most direct ways to prove our most likely scenario (that binary C is in Image 2) is to (i) check for binary C eclipses in Image 2, and/or (ii) check for RV motions in Image 2 with $P = 1.96$ d.

5.2 Outer Orbital Period Distribution

Armed with only the relative velocity between Image 1 and Image 2 projected onto the sky, $v_{\text{sky}} \simeq 5.7 \text{ km s}^{-1}$, and the projected separation on the sky, $s_{\text{sky}} \simeq 307 \text{ au}$, we attempt to estimate a probability distribution for the outer orbital period P_{out} via a Monte Carlo approach. Let \vec{s} and \vec{v} be the full relative position and velocity vectors between Image 1 and Image 2. In that case

$$\frac{s_{\text{sky}}}{s} = \sin \beta_1, \quad (4)$$

$$\frac{v_{\text{sky}}}{v} = \sin \beta_2, \quad (5)$$

where β_1 is the angle between the observer's view direction and \vec{s} and β_2 is the angle between the view direction and \vec{v} . If we know nothing about the orientation of the orbit on the sky, then samples of $\sin \beta$ can be drawn randomly from:

$$\sin \beta = \sqrt{1 - \mathcal{R}^2}, \quad (6)$$

where \mathcal{R} is a uniformly distributed random number between 0 and 1. Here, as an approximation, we treat \hat{s} and \hat{v} as independently and randomly directed with respect to the observer's view direction. So, we randomly draw β_1 and β_2 .

The energy of the outer orbit can now be written as

$$\mathcal{E} = -\frac{GM_1M_2}{s_{\text{sky}}} \sin \beta_1 + \frac{1}{2} \frac{M_1M_2}{M_{\text{ABC}}} \left(\frac{v_{\text{sky}}}{\sin \beta_2} \right)^2 = -\frac{GM_1M_2}{2a_{\text{out}}}, \quad (7)$$

where $M_1 \equiv M_A + M_B$ and $M_2 \equiv M_C$. This reduces to a simple expression for the semi-major axis of the outer orbit:

$$\frac{1}{a_{\text{out}}} = \frac{2 \sin \beta_1}{s_{\text{sky}}} - \left(\frac{v_{\text{sky}}}{GM_{\text{ABC}} \sin \beta_2} \right)^2. \quad (8)$$

Finally, we make a large number of random draws for β_1 and β_2 and, for each combination, store the realization for the semi-major axis and corresponding P_{out} . The resultant distribution for P_{out} is shown in Fig. 8. The distribution has a sharp cut at $\simeq 1500$ years, reflecting the fact that the minimum orbital separation is attained when $\beta_1 = \beta_2 = 90^\circ$, i.e., when the outer orbit is in the plane of the sky. However, since we do not know the orbital parameters in the line of sight, long orbital periods are possible, as evidenced by the long tail of the period distribution in Figure 8. The median of the orbital period distribution is close to 3000 years.

We note that our uncertain knowledge of the outer orbit could be greatly improved with a radial velocity study of Image 2 (which presumably hosts binary C).

5.3 Possible role of the 3:2 mean motion resonance

Zasche et al. (2019) presented a thorough analysis of stellar quadruple systems with a 2+2 architecture that exhibit eclipses of both components, with binary periods less than 15 days. One of the interesting population results from this study was the identification of a statistically significant group of systems having a period ratio close to 3/2. Zasche et al. (2019) speculated that these systems are either captured in the 3:2 mean motion resonance of the binary periods, or interacted with this resonance in the recent past and still reside close to it. One of the consequences for this class of systems would be a possible excitation of the orbital eccentricity of

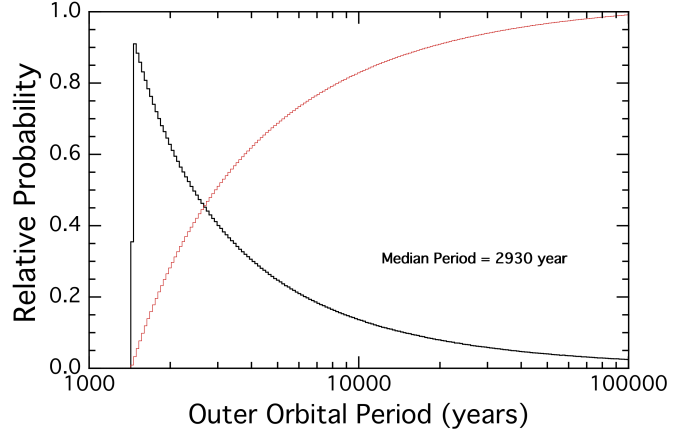


Figure 8. Probability distribution for the outer orbit of the V994 Her system. Results have been logarithmically binned. The black histogram is the differential probability distribution, while the red curve is the cumulative distribution.

the binary with the longer period. The V994 Her system was considered in this class by Zasche et al. (2019). Now, with much more detailed information about V994 Her, we revise its status with respect to the group of objects that reside or interacted with the 3:2 resonance in the past.

We use an analytical description of the low-order mean motion resonances in 2+2 quadruples by Tremaine (2020) (for completeness, see also Breiter & Vokrouhlický 2018, who discuss the 1:1 mean motion resonant states in the 2+2 quadruples). First, it is trivial to check that V994 Her is not currently located in the resonance since $1 - (2P_A/3P_B) \simeq 0.02204$ is too large (it would need to be three orders of magnitude smaller to be considered to possess this resonance). Tremaine (2020) also discusses sidebands of the pure 3:2 mean motion resonance between P_A and P_B generated by multiplets of the mean motion frequency n_{AB} of the mutual orbit. Their importance is typically very small, because the sideband width at frequency $k n_{\text{AB}}$ has a multiplicative factor $\propto e_{\text{AB}}^{|k|}$ (k is an integer). Here, $e_{\text{AB}} \simeq 0.7$ is a rather large value. However, to account for the three orders of magnitude in separation between the observed eccentricity and the requirement for resonance, $|k|$ would have to be greater than 30, which is much too large. The system, however, may have crossed the resonance in the past; this could have contributed to an excitation of the e_A value.

In order to place the system into the exact 3:2 mean motion resonance, one would need to (i) increase P_A by $\Delta P_A \simeq 0.046943$ day, (ii) decrease P_B by $\Delta P_B \simeq 0.031296$ day, or (iii) perform some combination of the two operations. Additionally, in order to temporarily capture V994 Her in the 3:2 resonance in the past, P_A and P_B should have been converging towards each other. In what follows, we shall discuss an end-member possibility (i) that P_B was constant, and P_A was evolving from an initially larger value beyond the resonance condition toward the current value. However, identical conclusions are obtained for other options, such as keeping P_A constant and P_B increasing as in (ii), or their combination.

Using the results from Appendix C of Tremaine (2020), we note that the putative past capture in the 3:2 resonance puts a severe constraint on the speed by which the period P_A

decreased. In particular, denoting the corresponding characteristic timescale $\tau_A = P_A/\dot{P}_A$ (with $\dot{P}_A = -dP_A/dt$), we find that

$$\tau_A \geq K (M_B/\mu_B)^{4/3} (a_{AB}/a_B)^{20/3} P_A, \quad (9)$$

where $K \simeq 1.74 \times 10^{-2}$, M_B and μ_B represent the total and reduced masses of the shorter period binary component, a_B and a_{AB} are the semimajor axes of the B and A-B orbits, and P_A is the orbital period of the A binary. Substituting the values from Table 3, we have $\tau_A \geq 26$ Gyr. Assuming an approximately steady decay of the A orbit, we then estimate a minimum time needed to accumulate the difference ΔP_A between the resonance and the current state

$$\Delta T_A \simeq \frac{\Delta P_A}{P_A} \tau_A \geq 580 \text{ Myr}. \quad (10)$$

This is nearly an order of magnitude longer than the estimated age of the V994 Her system (Table 3). Since other possibilities outlined above lead to the same result, such as P_B drifting toward its current value from an initially smaller value, we may conclude that the V994 Her system in all likelihood never interacted with the 3:2 mean motion resonance. Its location near to it might therefore be just coincidental. As a consequence, the e_A value is fully a relic of the initial state, with possible tidal damping. Indeed, the interaction with the 3:2 resonance would likely not be capable of explaining the significantly larger e_B value. The latter might be excited by interaction with the 2:1 mean motion resonance between P_A and P_B values; the location of this resonance, however, is much too distant from the current system parameters.

6 SUMMARY AND CONCLUSIONS

In this paper, we have demonstrated that the first-known doubly eclipsing system V994 Herculis is in fact at least a sextuple system that unambiguously demonstrates three sets of eclipses. Using *TESS* and archival data, we have disentangled the light curves of all three binaries in the system using three different techniques and added new measurements to the O–C diagrams of binaries A and B. We have also identified the period of the newly-discovered binary C to be 1.9601 days, based on *TESS* and older ground-based data. Finally, we used archival data from the Washington Double Star Catalog (spanning over 190 years) alongside parameters from Gaia DR3 in order to prove that the fainter visual companion on the night sky (1.1'' distant) is likely gravitationally bound to this system and may harbor binary C.

Depending on the nature of the companion star, this could be either a rare (2+2)+2 sextuple star system—similar to the well-known system Castor, with the same architecture (see, e.g., Stelzer & Burwitz 2003, and Tokovinin 2018). Another possibility is that the brighter star has six unresolvable stars, and the nearby visual companion is another bound member of the system, making it even more interesting—a potential septuple (or even higher-multiplicity) star system. Using additional data, we can more precisely derive the outer orbit; moreover, updated higher angular-resolution photometry would be able to firmly prove whether or not the C pair resides in the fainter nearby component. We urge the community to observe these interesting stars using the tools at their disposal. The high-angular separation techniques (both in photometry as well as spectroscopy) would be able to prove

the true structure of the system. As the separation of the visual pair on the night sky is slowly decreasing, it may become increasingly difficult to carry out these observations as time goes on.

DATA AVAILABILITY

The *TESS* data underlying this article were accessed using the MAST (Barbara A. Mikulski Archive for Space Telescopes) Portal (<https://mast.stsci.edu/portal/Mashup/Clients/Mast/Portal.html>). Some of the data were derived from sources in the public domain; their URLs are provided as footnotes. The derived data generated in this paper and the code used for the photodynamical analysis will be shared upon reasonable request to the corresponding author P.Z.

ACKNOWLEDGMENTS

This paper includes data collected by the *TESS* mission, specifically as part of GI program G022062 (PI: A. Prša). Funding for the *TESS* mission is provided by the NASA Science Mission Directorate. Resources used in this work were provided by the NASA High End Computing (HEC) Program through the NASA Advanced Supercomputing (NAS) Division at Ames Research Center for the production of the SPOC data products. Some of the data presented in this paper were obtained from the Mikulski Archive for Space Telescopes (MAST). STScI is operated by the Association of Universities for Research in Astronomy, Inc., under NASA contract NAS5-26555. Support for MAST for non-HST data is provided by the NASA Office of Space Science via grant NNX09AF08G and by other grants and contracts.

This research has made use of the Washington Double Star Catalog maintained at the U.S. Naval Observatory, and we thank Rachel Matson for providing archival data on the V994 Her visual double.

This work has used data from the European Space Agency (ESA) mission Gaia³, processed by the Gaia Data Processing and Analysis Consortium (DPAC)⁴. Funding for the DPAC is provided by national institutions, in particular those participating in the Gaia Multilateral Agreement.

Some of the observations in the paper made use of the High-Resolution Imaging instrument ‘Alopeke, obtained under Gemini LLP Proposal Number: GN/S-2021A-LP-105. ‘Alopeke was funded by the NASA Exoplanet Exploration Program and built at the NASA Ames Research Center by Steve B. Howell, Nic Scott, Elliott P. Horch, and Emmett Quigley. ‘Alopeke was mounted on the Gemini North (and/or South) telescope of the international Gemini Observatory, a program of NSF’s NOIR Lab, which is managed by the Association of Universities for Research in Astronomy (AURA) under a cooperative agreement with the National Science Foundation, on behalf of the Gemini partnership: the National Science Foundation (United States), National Research

³ <https://www.cosmos.esa.int/gaia>

⁴ <https://www.cosmos.esa.int/web/gaia/dpac/consortium>

Council (Canada), Agencia Nacional de Investigación y Desarrollo (Chile), Ministerio de Ciencia, Tecnología e Innovación (Argentina), Ministério da Ciência, Tecnologia, Inovações e Comunicações (Brazil), and Korea Astronomy and Space Science Institute (Republic of Korea).

This work is supported by MEYS (Czech Republic) under the projects MEYS LM2010105, LTT17006 and EU/MEYS CZ.02.1.01/0.0/0.0/16_013/0001403 and CZ.02.1.01/0.0/0.0/18_046/0016007.

M.B. and D.V. were supported by the Czech Science Foundation, grant GA21-11058S.

We also used the Simbad service operated by the Centre des Données Stellaires (Strasbourg, France) and the ESO Science Archive Facility services (data obtained under request number 396301).

REFERENCES

- Aarseth S. J., Mardling R. A., 2001, in Podsiadlowski P., Rappaport S., King A. R., D'Antona F., Burderi L., eds, *Astronomical Society of the Pacific Conference Series Vol. 229, Evolution of Binary and Multiple Star Systems*. p. 77 ([arXiv:astro-ph/0011514](https://arxiv.org/abs/astro-ph/0011514))
- Borkovits T., et al., 2011, *IBVS*, **5979**, 1
- Borkovits T., Hajdu T., Sztakovics J., Rappaport S., Levine A., Bíró I. B., Klagyivik P., 2016, *MNRAS*, **455**, 4136
- Borkovits T., et al., 2019, *MNRAS*, **483**, 1934
- Borkovits T., Rappaport S. A., Hajdu T., Maxted P. F. L., Pál A., Forgács-Dajka E., Klagyivik P., Mitnyan T., 2020, *MNRAS*, **493**, 5005
- Borkovits T., et al., 2021, *MNRAS*, **503**, 3759
- Breiter S., Vokrouhlický D., 2018, *MNRAS*, **475**, 5215
- Brož M., 2017, *ApJS*, **230**, 19
- Brož M., et al., 2022, *A&A*, **666**, A24
- Claret A., 2004, *A&A*, **424**, 919
- Claret A., 2007, *A&A*, **467**, 1389
- Claret A., Cunha N. C. S., 1997, *A&A*, **318**, 187
- Claret A., Giménez A., 2010, *A&A*, **519**, A57
- Cutri R. M., et al., 2021, *VizieR Online Data Catalog*, p. II/328
- Gaia Collaboration et al., 2022, arXiv e-prints, p. [arXiv:2208.00211](https://arxiv.org/abs/2208.00211)
- Howell S. B., Everett M. E., Sherry W., Horch E., Ciardi D. R., 2011, *AJ*, **142**, 19
- Jenkins J. M., et al., 2016, in Chiozzi G., Guzman J. C., eds, *Society of Photo-Optical Instrumentation Engineers (SPIE) Conference Series Vol. 9913, Software and Cyberinfrastructure for Astronomy IV*. p. 99133E, [doi:10.1117/12.2233418](https://doi.org/10.1117/12.2233418)
- Klinglesmith D. A., Sobieski S., 1970, *AJ*, **75**, 175
- Kozai Y., 1962, *AJ*, **67**, 591
- Kristiansen M. H. K., et al., 2022, *PASP*, **134**, 074401
- Lee C. U., Kim S. L., Lee J. W., Kim C. H., Jeon Y. B., Kim H. I., Yoon J. N., Humphrey A., 2008, *MNRAS*, **389**, 1630
- Lidov M. L., 1962, *Planet. Space Sci.*, **9**, 719
- Lucy L. B., 1967, *Z. Astrophys.*, **65**, 89
- Mardling R. A., Aarseth S. J., 2001, *MNRAS*, **321**, 398
- Martín-Ruiz S., et al., 2013, in Suárez J. C., Garrido R., Balona L. A., Christensen-Dalsgaard J., eds, *Astrophysics and Space Science Proceedings Vol. 31, Stellar Pulsations: Impact of New Instrumentation and New Insights*. p. P39
- Mason B. D., Wycoff G. L., Hartkopf W. I., Douglass G. G., Worley C. E., 2001, *AJ*, **122**, 3466
- Mikkola S., 2008, in Hubrig S., Petr-Gotzens M., Tokovinin A., eds, *Multiple Stars Across the H-R Diagram*. p. 11, [doi:10.1007/978-3-540-74745-1_2](https://doi.org/10.1007/978-3-540-74745-1_2)
- Pál A., 2012, *MNRAS*, **421**, 1825
- Pejcha O., Cagaš P., Landri C., Fausnaugh M. M., De Rosa G., Prieto J. L., Henzl Z., Pešta M., 2022, *A&A*, **667**, A53
- Plachy E., et al., 2021, *ApJS*, **253**, 11
- Powell B. P., et al., 2021, *AJ*, **161**, 162
- Prouza M., et al., 2019, in *36th International Cosmic Ray Conference (ICRC2019)*. p. 769, [doi:10.22323/1.358.0769](https://doi.org/10.22323/1.358.0769)
- Prša A., Zwitter T., 2005, *ApJ*, **628**, 426
- Rappaport S., Deck K., Levine A., Borkovits T., Carter J., El Mellah I., Sanchis-Ojeda R., Kalomeni B., 2013, *ApJ*, **768**, 33
- Ricker G. R., et al., 2015, *JATIS*, **1**, 014003
- Schmitt A. R., Hartman J. D., Kipping D. M., 2019, arXiv e-prints, p. [arXiv:1910.08034](https://arxiv.org/abs/1910.08034)
- Scott N. J., et al., 2021, *Frontiers in Astronomy and Space Sciences*, **8**, 138
- Stassun K. G., et al., 2019, *AJ*, **158**, 138
- Stelzer B., Burwitz V., 2003, *A&A*, **402**, 719
- Tokovinin A., 2018, *ApJS*, **235**, 6
- Tremaine S., 2020, *MNRAS*, **493**, 5583
- Vokrouhlický D., 2016, *MNRAS*, **461**, 3964
- Zahn J. P., 1977, *A&A*, **57**, 383
- Zasche P., Uhlař R., 2016, *A&A*, **588**, A121
- Zasche P., et al., 2019, *A&A*, **630**, A128

APPENDIX A: TABLE OF TIMES OF ECLIPSES

Table A1. *TESS* observed times of minima of V994 Her A

Eclipse Time BJD-2400000	Cycle no.	std. dev. (<i>d</i>)	Eclipse Time BJD-2400000	Cycle no.	std. dev. (<i>d</i>)	Eclipse Time BJD-2400000	Cycle no.	std. dev. (<i>d</i>)
59011.208388	0.0	0.000068	59393.510297	183.5	0.000244	59744.520841	352.0	0.000102
59012.282173	0.5	0.000038	59394.519437	184.0	0.000103	59745.592606	352.5	0.000108
59013.291644	1.0	0.000027	59395.593429	184.5	0.000134	59746.604119	353.0	0.000102
59014.365223	1.5	0.000039	59396.602611	185.0	0.000128	59747.675710	353.5	0.000085
59015.375104	2.0	0.000028	59397.676809	185.5	0.000113	59748.686773	354.0	0.000100
59016.448767	2.5	0.000038	59398.686003	186.0	0.000110	59749.759375	354.5	0.000097
59017.458488	3.0	0.000028	59399.760013	186.5	0.000116	59750.770102	355.0	0.000093
59018.532198	3.5	0.000044	59400.769258	187.0	0.000105	59751.842493	355.5	0.000101
59019.541632	4.0	0.000028	59401.843411	187.5	0.000115	59752.853041	356.0	0.000097
59020.615100	4.5	0.000036	59402.852513	188.0	0.000098	59753.926086	356.5	0.000109
59021.624954	5.0	0.000030	59403.926596	188.5	0.000173	59754.937116	357.0	0.000153
59023.708034	6.0	0.000040	59407.018862	190.0	0.000150	59757.020019	358.0	0.000086
59025.791322	7.0	0.000031	59408.093094	190.5	0.000142	59759.103225	359.0	0.000084
59027.874755	8.0	0.000029	59410.176195	191.5	0.000125	59760.175520	359.5	0.000103
59028.948286	8.5	0.000040	59411.185709	192.0	0.000125	59761.186560	360.0	0.000087
59029.957752	9.0	0.000028	59412.259529	192.5	0.000132	59762.259204	360.5	0.000102
59031.031620	9.5	0.000041	59413.268755	193.0	0.000107	59763.269832	361.0	0.000082
59032.041094	10.0	0.000030	59414.342947	193.5	0.000129	59764.342122	361.5	0.000094
59033.114938	10.5	0.000039	59415.352144	194.0	0.000113	59765.353549	362.0	0.000092
59034.124636	11.0	0.000032	59416.426295	194.5	0.000120	59766.426020	362.5	0.000132
59391.426417	182.5	0.004700	59417.435270	195.0	0.000112	59767.436725	363.0	0.000098
59392.436550	183.0	0.000110	59418.509214	195.5	0.000165	59768.508944	363.5	0.000190

Table A2. *TESS* observed times of minima of V994 Her B

Eclipse Time BJD-2400000	Cycle no.	std. dev. (<i>d</i>)	Eclipse Time BJD-2400000	Cycle no.	std. dev. (<i>d</i>)	Eclipse Time BJD-2400000	Cycle no.	std. dev. (<i>d</i>)
59010.698099	0.0	0.000046	59392.097175	268.5	0.000104	59418.259993	287.0	0.000104
59011.515257	0.5	0.000044	59392.700110	269.0	0.000111	59744.251213	516.5	0.000111
59012.118117	1.0	0.000041	59393.517972	269.5	0.000156	59744.855372	517.0	0.000121
59012.934955	1.5	0.000038	59394.119951	270.0	0.000103	59745.671247	517.5	0.000131
59013.537998	2.0	0.000042	59394.936970	270.5	0.000111	59746.274246	518.0	0.000112
59014.355223	2.5	0.000040	59395.539982	271.0	0.000149	59747.092093	518.5	0.000150
59014.957744	3.0	0.000046	59396.357565	271.5	0.000083	59747.695762	519.0	0.000105
59015.774811	3.5	0.000043	59396.960021	272.0	0.000105	59748.511739	519.5	0.000095
59016.377966	4.0	0.000042	59397.776849	272.5	0.000149	59749.114405	520.0	0.000130
59017.194853	4.5	0.000039	59398.379989	273.0	0.000117	59749.931728	520.5	0.000125
59017.798052	5.0	0.000041	59399.197749	273.5	0.000093	59750.535692	521.0	0.000125
59018.614518	5.5	0.000035	59399.800066	274.0	0.000158	59751.351793	521.5	0.000074
59019.218026	6.0	0.000041	59400.617105	274.5	0.000128	59751.954686	522.0	0.000141
59020.035181	6.5	0.000040	59401.219664	275.0	0.000102	59752.771888	522.5	0.000125
59020.638250	7.0	0.000041	59402.037976	275.5	0.000125	59753.376286	523.0	0.000101
59021.455270	7.5	0.000042	59402.640244	276.0	0.000103	59754.192150	523.5	0.000128
59022.058251	8.0	0.000047	59403.457233	276.5	0.000109	59754.794952	524.0	0.000153
59023.478273	9.0	0.000047	59404.059974	277.0	0.000109	59755.612006	524.5	0.000110
59024.295584	9.5	0.000043	59405.480590	278.0	0.000133	59757.032126	525.5	0.000142
59024.898039	10.0	0.000047	59406.297671	278.5	0.000102	59757.634921	526.0	0.000116
59025.715847	10.5	0.000044	59406.900386	279.0	0.000163	59758.452032	526.5	0.000112
59026.318513	11.0	0.000048	59407.718358	279.5	0.000116	59759.055882	527.0	0.000183
59027.136039	11.5	0.000051	59408.320651	280.0	0.000110	59759.872291	527.5	0.000123
59027.738752	12.0	0.000044	59409.137946	280.5	0.000172	59760.475192	528.0	0.000116
59028.555943	12.5	0.000043	59409.740282	281.0	0.000106	59761.291883	528.5	0.000129
59029.158935	13.0	0.000039	59410.558443	281.5	0.000107	59761.895816	529.0	0.000116
59029.975931	13.5	0.000043	59411.160938	282.0	0.000165	59762.712201	529.5	0.000123
59030.578838	14.0	0.000042	59411.977957	282.5	0.000112	59763.315197	530.0	0.000126
59031.395642	14.5	0.000044	59412.580171	283.0	0.000096	59764.132083	530.5	0.000106
59031.998690	15.0	0.000045	59413.397720	283.5	0.000171	59764.735789	531.0	0.000140
59032.815480	15.5	0.000042	59414.000752	284.0	0.000117	59765.552266	531.5	0.000117
59033.418734	16.0	0.000045	59414.817875	284.5	0.000108	59766.155117	532.0	0.000126
59034.235331	16.5	0.000040	59415.420146	285.0	0.000182	59766.972072	532.5	0.000101
59034.838698	17.0	0.000044	59416.238006	285.5	0.000118	59767.575534	533.0	0.000120
59390.677560	267.5	0.000177	59416.840945	286.0	0.000127	59768.392581	533.5	0.000089
59391.279999	268.0	0.000108	59417.658130	286.5	0.000136			

Table A3. *TESS* observed times of minima of V994 Her C

Eclipse Time BJD-2400000	Cycle no.	std. dev. (<i>d</i>)	Eclipse Time BJD-2400000	Cycle no.	std. dev. (<i>d</i>)	Eclipse Time BJD-2400000	Cycle no.	std. dev. (<i>d</i>)
59011.124177	0.0	0.000157	59392.220634	194.5	0.002012	59418.829817	208.0	0.000596
59011.953279	0.5	0.000895	59393.348483	195.0	0.000439	59744.209501	374.0	0.001378
59013.083475	1.0	0.000176	59394.181279	195.5	0.001782	59746.169255	375.0	0.000467
59013.916603	1.5	0.000925	59395.308080	196.0	0.000453	59746.993487	375.5	0.002726
59015.045185	2.0	0.000170	59396.130606	196.5	0.002677	59748.129163	376.0	0.000505
59015.878338	2.5	0.000773	59397.270147	197.0	0.000509	59748.960592	376.5	0.002910
59017.005797	3.0	0.000173	59398.082565	197.5	0.007348	59750.091678	377.0	0.000459
59017.835692	3.5	0.000770	59399.229029	198.0	0.000449	59750.911553	377.5	0.016446
59018.965311	4.0	0.000174	59401.187681	199.0	0.000375	59752.050606	378.0	0.000432
59019.796083	4.5	0.001014	59402.019831	199.5	0.007591	59752.873428	378.5	0.057992
59020.925121	5.0	0.000169	59403.148862	200.0	0.000397	59754.009831	379.0	0.000405
59021.753129	5.5	0.001266	59403.972393	200.5	0.003418	59754.822117	379.5	0.003540
59023.720603	6.5	0.001604	59405.927779	201.5	0.004661	59755.972515	380.0	0.000694
59024.845884	7.0	0.000172	59407.069016	202.0	0.000706	59757.931960	381.0	0.000433
59025.682738	7.5	0.001401	59407.894095	202.5	0.057096	59758.756173	381.5	0.005398
59026.806343	8.0	0.000171	59409.028342	203.0	0.000656	59759.890913	382.0	0.000483
59027.640483	8.5	0.000943	59409.856410	203.5	0.002463	59760.706877	382.5	0.010731
59028.767693	9.0	0.000186	59410.989522	204.0	0.000463	59761.850436	383.0	0.000442
59029.597642	9.5	0.001409	59411.812507	204.5	0.003274	59762.669061	383.5	0.003683
59030.727133	10.0	0.000175	59412.949612	205.0	0.000503	59763.811861	384.0	0.000536
59031.559275	10.5	0.000946	59414.908974	206.0	0.000444	59764.636994	384.5	0.001506
59032.688509	11.0	0.000180	59415.758940	206.5	0.002578	59765.771756	385.0	0.000524
59033.522849	11.5	0.001363	59416.870114	207.0	0.000460	59767.732579	386.0	0.000409
59034.648313	12.0	0.000173	59417.696368	207.5	0.001980	59768.560018	386.5	0.007387
59391.388607	194.0	0.000580						

Table A4. New, unpublished eclipse times of V994 Her for binaries A, B, and C.

Eclipse Time BJD-2400000	std. dev. (<i>d</i>)	Pair [A/B/C]	Type [P/S]	Reference/ Observer	Eclipse Time BJD-2400000	std. dev. (<i>d</i>)	Pair [A/B/C]	Type [P/S]	Reference/ Observer
57843.57013	0.00045	A	S	R.U.	59802.47556	0.00045	B	S	R.U.
57855.59639	0.00073	B	S	R.U.	59804.49687	0.00048	B	P	R.U.
57902.45775	0.00069	B	S	R.U.	59815.34773	0.00192	A	P	R.U.
57916.48823	0.00185	A	S	R.U.	59816.42734	0.00148	A	S	R.U.
57917.49528	0.00029	A	P	R.U.	59817.43375	0.00030	A	P	R.U.
57940.40624	0.00014	A	P	R.U.	59817.43433	0.00036	A	P	FRAM
57946.48532	0.00097	B	S	R.U.	59818.50532	0.00052	A	S	FRAM
57968.38272	0.00099	B	P	R.U.	59121.62037	0.00054	A	P	G.P.
58232.53401	0.00037	B	P	R.U.	52509.78153	0.00211	B	P	S.D. & U.M.
58257.48416	0.00075	B	S	R.U.	52510.52766	0.00651	B	S	S.D. & U.M.
58290.38397	0.00021	A	P	R.U.	52702.91006	0.00275	B	P	S.D. & U.M.
58343.53778	0.00079	A	S	R.U.	52703.66135	0.00066	B	S	S.D. & U.M.
58387.30392	0.00032	B	P	R.U.	52810.86153	0.00098	B	P	S.D. & U.M.
58565.62065	0.00055	B	S	R.U.	52811.60611	0.00190	B	S	S.D. & U.M.
58570.62894	0.00082	A	S	R.U.	53096.26742	0.00274	B	P	S.D. & U.M.
58571.63882	0.00069	A	P	R.U.	53097.02123	0.00193	B	S	S.D. & U.M.
58593.55169	0.00068	A	S	R.U.	53171.53199	0.00181	B	P	S.D. & U.M.
58614.50216	0.00135	B	P	R.U.	53172.28521	0.00092	B	S	S.D. & U.M.
58667.47186	0.00029	A	P	R.U.	52692.65792	0.00048	A	P	S.D. & U.M.
58689.37993	0.00062	A	S	R.U.	52715.57549	0.00129	A	P	S.D. & U.M.
58957.55352	0.00149	B	S	R.U.	53139.55537	0.00089	A	S	S.D. & U.M.
58991.45731	0.00075	A	S	R.U.	52509.33511	0.00026	A	P	S.D. & U.M.
59023.47973	0.00039	B	P	R.U.	52510.40944	0.00040	A	S	S.D. & U.M.
59043.52943	0.00062	A	S	R.U.	52735.40298	0.00091	A	S	S.D. & U.M.
59040.37413	0.00091	A	P	R.U.	52825.97834	0.00148	A	P	S.D. & U.M.
59040.52213	0.00085	B	P	R.U.	52827.05749	0.00202	A	S	S.D. & U.M.
59089.36019	0.00045	A	S	R.U.	53102.05902	0.00052	A	S	S.D. & U.M.
59102.40213	0.00043	B	S	R.U.	53171.80904	0.00057	A	P	S.D. & U.M.
59343.51031	0.00033	A	S	R.U.	52687.49036	0.00950	A	S	S.D. & U.M.
59349.50020	0.00025	B	S	R.U.	59831.47733	0.00027	B	P	FRAM
59361.46286	0.00064	B	P	FRAM	59840.35162	0.00046	A	P	R.U.
59367.43420	0.00017	A	P	R.U.	54669.45443	0.00100	C	P	MR13
59369.51977	0.00030	A	P	M.M.	59101.29077	0.00531	C	P	R.U.
59392.43409	0.00019	A	P	R.U.	59150.29198	0.00134	C	P	R.U.
59416.42568	0.00040	A	S	FRAM	59152.25463	0.00389	C	P	R.U.
59419.52306	0.00038	A	P	R.U.	59279.67396	0.00770	C	P	R.U.
59425.36003	0.00070	B	P	R.U.	59332.58531	0.00473	C	P	R.U.
59463.27078	0.00245	A	P	R.U.	59338.46323	0.00633	C	P	R.U.
59465.35947	0.00037	A	P	R.U.	59436.47808	0.00354	C	P	R.U.
59677.51573	0.00055	B	S	R.U.	59438.44039	0.00257	C	P	R.U.
59679.53400	0.00044	B	P	R.U.	59497.24210	0.01257	C	P	R.U.
59717.43638	0.00055	A	P	R.U.	59675.60538	0.00101	C	P	R.U.
59718.50933	0.00034	A	S	R.U.	59681.49018	0.00107	C	P	R.U.
59742.43700	0.00079	A	P	R.U.	59779.49300	0.00100	C	P	R.U.
59767.43486	0.00021	A	P	R.U.	52819.10680	0.00232	C	P	S.D. & U.M.
59767.57676	0.00069	B	P	R.U.	52693.65303	0.00273	C	P	S.D. & U.M.
59775.49098	0.00054	B	S	R.U.	59828.49557	0.00325	C	P	FRAM
59787.45377	0.00079	B	P	R.U.	59830.45265	0.00304	C	P	FRAM
59791.42428	0.00071	A	S	R.U.					

Notes: G.P. = Gerald Persha, see <http://var2.astro.cz>; S.D. & U.M. = S. Dallaporta & U.Munari; R.U. = R.Uhlař; M.M. = M.Mašek; MR13 = [Martín-Ruiz et al. \(2013\)](#)